

# Curvature Potential Formulation for Thin Elastic Sheets

Yael Cohen,<sup>1</sup> Animesh Pandey,<sup>2</sup> Yafei Zhang,<sup>1</sup> Cy Maor,<sup>3</sup> and Michael Moshe<sup>1,\*</sup>

<sup>1</sup>*Racah Institute of Physics, The Hebrew University of Jerusalem, Jerusalem, Israel*

<sup>2</sup>*Engineering Mechanics Unit, Jawaharlal Nehru Center for Advanced Scientific Research, Bengaluru, India*

<sup>3</sup>*Einstein Institute of Mathematics, The Hebrew University of Jerusalem, Jerusalem, Israel*

Thin elastic sheets appear in systems ranging from graphene to biological membranes, where phenomena such as wrinkling, folding, and thermal fluctuations originate from geometric nonlinearities. These effects are treated within weakly nonlinear theories, such as the Föppl–von Kármán equations, which require small slopes and fail when deflections become large even if strains remain small. We introduce a methodological progress via a geometric reformulation of thin-sheet elasticity based on a stress potential and a curvature potential. This formulation preserves the structure of the classical equations while extending their validity to nonlinear, multivalued configurations, and geometrically frustrated states. The framework provides a unified description of thin-sheet mechanics in regimes inaccessible to existing theories and opens new possibilities for the study of elastic membranes and two-dimensional materials.

**Introduction.** The physics of thin elastic sheets is central to a broad range of condensed-matter systems [1–3], from graphene, whose electronic properties are exquisitely strain-dependent [4, 5], to biological membranes, including tissues and plant leaves [6–10]. Yet, thin sheets elasticity constitutes a geometrically nonlinear field theory which makes the theory analytically challenging, and continues to impede theoretical progress [11, 12]. To make analytical progress, one typically resorts to controlled approximation schemes. A classical reduction is obtained by expressing a deformed surface through an in-plane displacement field  $\mathbf{d}$  and a height function  $f$  describing flexural deflections relative to a reference surface, and assuming a scaling relation between the different deformation modes. In the weakly nonlinear regime, for example, where  $|\nabla \mathbf{d}| \sim |\nabla f|^2 \ll 1$ , one arrives at the well-known nonlinear Föppl-von Kármán (FvK) theory [13, 14].

This approach has enjoyed substantial success: it underlies the renormalization of elastic moduli in thermally fluctuating membranes [15–18], the mechanics and geometry of defective crystalline monolayers [19, 20], and the extreme behaviors of wrinkling, crumpling, and other phenomena in natural and synthetic slender solids [21–26]. Despite these achievements, the approach suffers from inherent limitations: beyond the basic assumption on small strains, it is restricted to small slopes and, crucially, to configurations that can be represented as a height function relative to a reference surface (aka Monge gauge). Prototypical configurations of practical relevance, from kirigami-inspired architectures [27] to graphene monolayers [20], often possess low elastic energy yet nonetheless violate these prerequisites, as illustrated in Fig. 1 for deformations of elastic ribbons and sheets. The twisted ribbon in Fig. 1(a), for instance, exhibits large slopes and cannot be represented by a single-valued height function, even though its elastic energy density is small for small twist per unit length. Analyzing such configurations typically requires returning to the full for-

mulation in terms of the configuration [17].

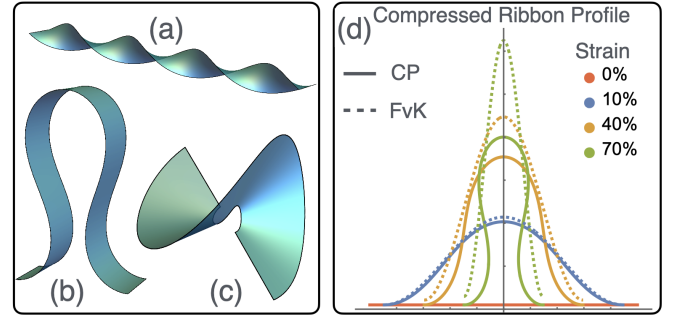


FIG. 1. Left: Curvature-potential-based analytical solutions for deformations that cannot be represented as a single-valued height function: (a) twisted ribbon, (b) compressed ribbon, and (c) bent sliced annulus. Right: Comparison between curvature-potential predictions (solid lines), and classical FvK interpretations (dashed). The curvature-potential formulation remains accurate even beyond 70% strain.

In this Letter, we introduce a fully intrinsic geometric formulation of thin-sheet elasticity that applies seamlessly to configurations with large slopes or multi-valued height functions, as presented in Fig. 1(a-c). This approach preserves the mathematical structure of previous frameworks, and provides a unified reinterpretation of previously studied problems. Crucially, it enables these analyses to be generalized to complex geometries, boundary conditions, and geometric frustration, that lie outside the reach of standard weakly nonlinear theories.

At the heart of our approach are two scalar fields: the classical Airy stress potential  $\chi$  (SP), from which the stress tensor is derived, and a curvature potential  $\psi$  (CP), which generates the curvature tensor of the surface. We show that, upon expressing the equilibrium equations in terms of these potentials and identifying the proper scaling relations between stretching and bending modes, one arrives at equilibrium equations that coincide in form with those of established theories, most notably FvK,

yet the field  $\psi$  no longer coincides with the classical interpretation as a normal deflection.

This distinction is illustrated in Fig. 1(d), showing different interpretations of the *same* elastic-ribbon solution expressed through our CP formulation (solid line) and the FvK interpretation (dashed). The analytic solutions for twisting and bending shown in Fig. 1(b-c) have no analogous configurations within the FvK framework.

In what follows we present the geometric formulation in terms of stress and curvature potentials, apply it to configurations beyond current frameworks, and demonstrate how it broadens the scope of earlier analyses. To validate our approach we complement the analytical results with numeric finite-element solution of the full problem and show excellent agreement. We conclude by discussing the implementation of our approach to a range of problems, including statistical physics of elastic membranes with large deformations and open problems in mechanics, as well as future directions.

**The Theoretical Framework.** Our starting point is the kinematic description of the configuration in 3D,  $\phi(u, v) = \{X(u, v), Y(u, v), Z(u, v)\}$ . Within the geometric approach to elasticity, the metric  $a_{\alpha\beta} = \partial_\alpha \phi \cdot \partial_\beta \phi$  encodes infinitesimal distances between nearby points on the surface, and the curvature tensor  $b_{\alpha\beta} = -\partial_\alpha \mathbf{n} \cdot \partial_\beta \phi$  encodes the relative orientation of surface normal  $\mathbf{n}$ . The elastic energy penalizes deviations of these fields from their reference values  $(\bar{a}, \bar{b})$ , leading to the standard functional with stretching and bending terms

$$E = \int \left[ \frac{h}{2} \mathcal{A}^{\alpha\beta\gamma\delta} \epsilon_{\alpha\beta}^{\text{st}} \epsilon_{\gamma\delta}^{\text{st}} + \frac{h^3}{6} \mathcal{A}^{\alpha\beta\gamma\delta} \epsilon_{\alpha\beta}^{\text{bn}} \epsilon_{\gamma\delta}^{\text{bn}} \right] dS, \quad (1)$$

$$\epsilon^{\text{st}} = \frac{1}{2}(a - \bar{a}), \quad \epsilon^{\text{bn}} = \frac{1}{2}(b - \bar{b}).$$

Although the reference fields  $\bar{a}$  and  $\bar{b}$  are independent, the actual fields  $a$  and  $b$  arise from an embedding  $\phi$ . They are therefore constrained by the Gauss and Mainardi-Peterson-Codazzi (MPC) compatibility conditions,

$$K_G(a) = \det(a^{-1}b), \quad \nabla \times b = 0, \quad (2)$$

which guarantee the local realizability of  $a$  and  $b$  by a surface in  $\mathbb{R}^3$ . The first relation is Gauss' classical *theorema egregium*, equating the intrinsic Gaussian curvature to its extrinsic expression through the shape operator  $s = a^{-1}b$ . The second condition expresses the integrability of the normal field for a configuration in  $\mathbb{R}^3$ .

The equilibrium equations may be obtained either by minimizing the functional (1) with respect to the embedding  $\phi(u, v)$ , or, assuming the elastic body is simply-connected, by a constrained minimization with respect to the fields  $a$  and  $b$  subject to (2). In either case, one arrives at the apparently compact system [12]

$$\begin{aligned} 0 &= \text{div}_{\bar{a},a} \Sigma + \text{div}_{\bar{a},a} m s, \\ 0 &= \text{div}_{\bar{a}} (\text{div}_{\bar{a},a} m) - \Sigma b, \end{aligned} \quad (3)$$

where  $\Sigma = \sigma + m s$ , is an effective stress combining stretching and bending contributions, with the stress  $\sigma$  and bending moment  $m$  linear in the corresponding strains  $\epsilon^{\text{st}}$  and  $\epsilon^{\text{bn}}$ , and the operator  $\text{div}_{\bar{a}}$  is the covariant divergence with respect to  $\bar{a}$  (see App. B). A key difficulty is that the differential operator  $\text{div}_{\bar{a},a}$  itself depends on the unknown metric  $a$  and on  $\bar{a}$ , making the system nonlinear and implicit.

These equations, when expressed in terms of  $a$  and  $b$ , must be supplemented by the compatibility constraints (2); only then does the system form a closed set for the unknown fundamental forms. These geometric constraints are automatically enforced when working directly with the in-plane displacement and normal deflection, as in the classical FvK formulation. In contrast, our intrinsic formulation keeps  $a$  and  $b$  as the primary variables, making the compatibility relations an explicit and essential part of the theory.

The central idea underlying our approach is to solve the compatibility equations *without* specifying an embedding  $\phi$  or a height function. This is made possible by introducing a scalar CP that automatically generates curvature fields consistent with MPC compatibility. The construction is valid whenever stretching and bending energies remain small, regardless of whether the resulting configuration can be represented as a height function or involves large slopes. While the framework applies more broadly, for concreteness and clarity we restrict attention here to cases in which  $\bar{a}$  is close to Euclidean and  $\bar{b} = 0$  (see App. B).

We note that any curvature tensor  $b$  that satisfies the MPC compatibility condition in Eq. (2) with Euclidean  $a$  can be expressed as  $b_{\alpha\beta} = \nabla_{\alpha\beta} \psi$ . Correspondingly, in cases of small strains this representation is valid as an approximation to first order in  $\epsilon^{\text{st}}$

$$b_{\alpha\beta} = \bar{\nabla}_{\alpha\beta} \psi. \quad (4)$$

In this approximation, the divergence operators in (3) simplify to  $\text{div}_{\bar{a}}$ , and assuming small bending strains the in-plane equilibrium equation reduces to  $\text{div}_{\bar{a}} \Sigma = 0$ . This equation is solved identically by introducing a generalized Airy stress potential (SP),  $\Sigma = \bar{\nabla} \times \bar{\nabla} \times \chi$  as in [28]. The remaining conditions are the Gauss compatibility relation in (2) and the bending-moment equation in (3), whose precise form depends on the scaling between stretching and bending strains,  $\epsilon_{\text{st}}$  and  $\epsilon_{\text{bn}}$ .

A generic case of interest is the regime in which stretching and bending contribute comparably to the total elastic energy. This corresponds to the scaling  $\epsilon_{\text{st}} \sim h \epsilon_{\text{bn}}$ . The classical FvK regime is recovered when  $\epsilon_{\text{bn}} \sim h \ell^{-2}$  where the length-scale  $\ell$  depends on the specific problem (see App. E). The equilibrium equations take the form:

$$Y^{-1} \bar{\Delta} \bar{\Delta} \chi = \det(\bar{a}^{-1}b) - \bar{K}_G \quad (5)$$

$$Y h^3 \bar{\Delta} \bar{\Delta} \psi = 12(1 - \nu^2) \sigma^{\alpha\beta} b_{\alpha\beta}. \quad (6)$$

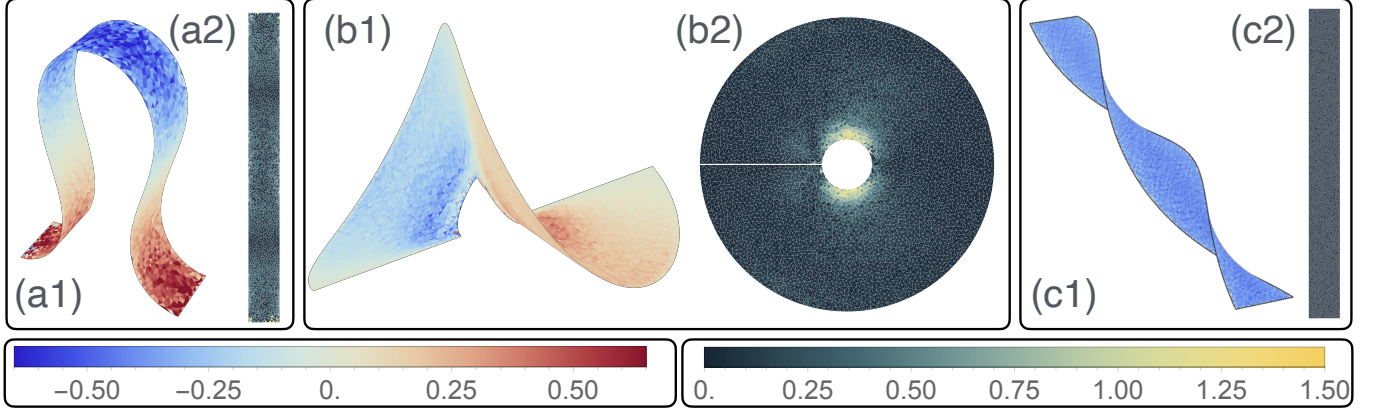


FIG. 2. Equilibrium configurations obtained from finite-element simulations and comparison with the curvature fields predicted by the CP formulation, all shown in the Lagrangian frame. (a1) Compressed ribbon of dimensions  $L = 10$ ,  $W = 1$  and thickness  $h = 0.05$ , subjected to compression. (b1) Bent sliced annulus, of radius  $R = 3$  and  $h = 0.04$ . (c1) Twisted ribbon of dimensions  $L = 10$ ,  $W = 1$  and  $h = 0.01$ . The compressed ribbon and the sliced annulus are colored by mean curvature, and the twisted ribbon by Gaussian curvature. The relative mean-curvature deviation  $(H_{FE} - H_{CP}) / \max(H_{CP})$  is shown in (a2) and (b2), and the relative Gaussian deviation  $1 - K_{FE}/K_{CP}$  is shown in (c2).

These equations coincide in form with the covariant FvK equations, with the crucial distinction that  $\psi$  is a CP rather than a configurational height function. Other scaling assumptions modify these equations. For example, in the thin limit where  $a = \bar{a}$  the stress in (6) take the role of a Lagrange multiplier enforcing isometry (see App. D).

Equations (5) and (6) are supplemented with the appropriate boundary conditions on the stress and bending moment (see App. C). With these in place, the reconstruction of the surface configuration proceeds in a manner fundamentally different from the classical approach. Given a solution for the potentials, the curvature tensor is obtained directly from  $\psi$  through Eq. (4), while the metric field  $a$  follows from  $a = \bar{a} + 2A\sigma$ , where  $A$  is the elastic tensor and the stress  $\sigma$  is  $\sigma \approx \bar{\nabla} \times \bar{\nabla} \times \chi$ .

The equations determining the configuration from the fundamental forms are the classical Weingarten equations [29]. Defining the tangent vectors  $\mathbf{t}_\alpha = \partial_\alpha \phi$  and the unit normal  $\mathbf{n}$ , this orthonormal triad satisfies

$$\begin{aligned} \partial_\alpha \mathbf{n} &= -b^\mu_\alpha \mathbf{t}_\mu \\ \partial_\alpha \mathbf{t}_\beta &= \Gamma^\mu_{\alpha\beta} \mathbf{t}_\mu + b_{\alpha\beta} \mathbf{n} \end{aligned} \quad (7)$$

where  $\Gamma$  is the Levi-Civita connection associated with  $a$  [29]. Solving this system yields the fields  $\{\mathbf{t}_1, \mathbf{t}_2, \mathbf{n}\}$ , from which the surface embedding  $\phi(u, v)$  is recovered by integration. Thus, once the potentials  $\chi$  and  $\psi$  are known, the fundamental forms  $a$  and  $b$  are reconstructed, and the configuration follows from integrating the Weingarten system. It is worth noting that when the surface admits a Monge-gauge representation  $z = f(u, v)$ , the small slope approximation identifies the deflection field  $f$  with the CP  $\psi$ .

**The Curvature Potential in Action** We illustrate the curvature-potential framework through three

prototypical systems: a clamped compressed ribbon, a twisted ribbon, and a sliced annulus. These geometries span a broad range of deformation modes, and provide representative tests for situations in which the classical displacement-based description becomes inadequate. While our framework applies to non-Euclidean plates and shells, in the current paper we focus on the effect of boundary conditions in cases with Euclidean reference metric, and leave more general cases for future work, as discussed in the summary section.

To benchmark the theory, we compare our predictions with full finite-element simulations of the elastic energy (1). In the simulations the sheet is discretized into a triangulated mesh, each triangle carrying its target metric, target curvature, thickness, and elastic moduli. From a given configuration we compute the actual metric and curvature, evaluate the corresponding energy, and relax the shape subject to prescribed boundary conditions (see App. A). These simulations serve as a quantitative reference for strongly nonlinear regimes that lie beyond the reach of classical analytical approaches.

**Compressed ribbon.** A long, narrow ribbon compressed between clamped ends provides the classical Euler-buckling scenario, relevant from thermalized graphene sheets to polymer ribbons. While the FvK equations successfully describe the buckling threshold and the weakly post-buckled regime, they cease to apply under strong compression where slopes become large and the configuration is no longer representable as a height graph [30]. For a ribbon with  $h \ll W \ll L$  and end separation  $\ell < L$ , whose clamped ends are held a distance  $\ell < L$ , the FvK solution takes the form

$$\chi(u, v) = \frac{Yh^3}{24(1-\nu^2)} \kappa^2 u^2, \quad \psi(u, v) = A \cos(\kappa u),$$

For a clamped ribbon, meaning the short edges held flat  $\kappa = \frac{2\pi}{L}n$ , for small force, we consider the lowest mode. The distance between those edges determines  $A$  (see App. C). with  $\kappa$  and  $A$  determined by boundary conditions (For more general solutions see App. F). Classically,  $\psi$  is interpreted as an out-of-plane deflection. In our framework the same functional form appears, but  $\psi$  is a CP rather than a height function.

This distinction leads to strikingly different reconstructed shapes. In Fig. 1(d) we show the profile of the configurations obtained when  $\psi$  is treated as a CP and integrated through the Weingarten equations (solid line), versus a height function (dashed line). While the classical approach typically fails at strains of order 10%, we now show that our approach remains accurate even at strains as high as 70% (i.e.,  $\ell = 0.3L$ ): Detailed comparison with full finite-element solution is shown in Fig. 2(a), where (a1) shows the configuration colored by mean curvature, and (a2) shows a practically vanishing difference between the analytic and numeric values of the mean curvature over the whole ribbon in the Lagrangian frame.

**Twisted ribbon.** Twisted ribbons appear in contexts ranging from graphene twist rigidity [31, 32] to self-assembly and wrinkling in stretched ribbons [22, 23]. Here the ribbon ends remain separated by distance  $\ell = L$  but are rotated about the centerline, producing a family of helicoidal configurations. The system and boundary conditions in this case suggests that the SP and CP depend only on the longitudinal coordinate  $u$ . Indeed, the solution of Eqs. (5) is

$$\chi(u, v) = -\frac{\gamma}{24}\psi_1 v^4, \quad \psi(u, v) = \psi_1 uv, \quad (8)$$

with  $\psi_1$  equal to the imposed twist per unit length. For more general solutions including additional boundary degrees of freedom see App. E.

The reconstructed surface corresponding to (8) is shown in Fig. 1(a), and features uniform nonzero Gaussian curvature and vanishing mean curvature. Accordingly, comparison of the analytic solution with full finite-element solution is shown in Fig. 2(c), where (c1) shows the configuration colored by Gaussian curvature, and (c2) shows the difference between the analytic and numeric values of the Gaussian curvature over the whole ribbon.

**Sliced annulus.** Lastly, we examine an annulus with a radial cut, where the opening angle and the relative tilt between the free edges can be prescribed independently. This geometry is of relevance to the mechanics of conical surfaces [33–35], and form a basic mechanism in kirigami [27] and origami [36]. Assuming curvature only on the azimuthal direction (see App. G):

$$\begin{aligned} \chi(r, \theta) &= a_1 \cos(2\theta) + a_2 \sin(2\theta) + r\theta(b_1 \cos \theta + b_2 \sin \theta), \\ \psi(r, \theta) &= r\theta(c_1 \cos \theta + c_2 \sin \theta), \end{aligned} \quad (9)$$

with the constants  $a_i, b_i, c_i$  set by boundary conditions. An example of a resulting configuration (with  $\chi = 0$ ) is shown in Fig. 1(c).

A comparison between the analytic and finite-element solutions is shown in Fig. 2(b). In (b1) the equilibrium configuration is colored by mean curvature, and in (b2) by the difference between the analytic and numeric values of the mean curvature over the whole ribbon. Note that a basic assumption in our current work is that  $\eta \equiv \epsilon_{st}/(h\epsilon_{bn})$  is of order one. To verify its validity, we calculate this expression for the determinants of the strains and find that in all cases  $\eta \sim 1 - 10$ .

**Summary and Discussion** We introduced an intrinsic curvature potential formulation of thin sheet elasticity that bypasses the limitations of weakly nonlinear, graph based descriptions. Comparison with full finite element minimization across several prototypical examples demonstrates that the curvature potential approach remains accurate even under very large strains, in regimes where classical FvK type theories fail.

Because the formulation is derived directly from the geometric elastic energy, it extends immediately to sheets with non Euclidean reference metrics  $\bar{a}$  or finite reference curvature  $\bar{b}$ . This includes systems shaped by growth, plastic deformation, residual stress, or programmed geometry, where incompatibility plays a central mechanical role. These cases lie beyond the scope of the present work but represent natural directions for future extensions.

A key conceptual implication of our formulation is that any problem previously solved within the FvK framework can be reinterpreted within the potential formulation without loss of physical meaning for intrinsic geometric observables. In statistical physics of fluctuating membranes, quantities that depend on the curvature tensor, such as normal gradient correlations, retain their classical structure. For instance,  $\langle \partial_i \mathbf{n}(\mathbf{q}) \partial_j \mathbf{n}(\mathbf{q}) \rangle = \langle \bar{a}^{kl} b_{ik}(\mathbf{q}) b_{jl}(\mathbf{q}) \rangle$ , and this relation holds regardless of whether  $b$  is expressed in terms of a shallow height function or a curvature potential. In contrast, extrinsic observables such as roughness, which rely directly on height-height correlations, do not admit a direct analogue in our interpretation and may require a reformulation.

These considerations open the possibility of revisiting the mechanics and statistical physics of fluctuating membranes, including graphene and lipid bilayers, in regimes where large geometric deflections coexist with small strains, a setting in which existing theories are known to break down.

This formulation raises new geometric questions concerning the global structure of surfaces. In particular, solving the elastic problem on a periodic annular domain requires enforcing not only the local Gauss–MCP compatibility conditions but also global, topological compatibility relations that couple the fundamental forms around the periodic direction. By deriving these global constraints, we will be able to address the problem of a dislocated annulus and, in doing so, offer new insight into the finite energy hypothesis for dislocations [37, 38].

Overall, the curvature potential formulation provides



a unified geometric framework that bridges the gap between weakly nonlinear plate theories and the fully nonlinear geometry of thin sheets. It preserves the structure and intuition of classical approaches while extending their reach to multivalued, large slope, and non Euclidean configurations. We expect this framework to find broad application in architected materials, growth driven morphogenesis, kirigami and origami mechanics, and thermalized two dimensional materials, and to serve as a foundation for further developments in geometric elasticity.

---

\* michael.moshe@mail.huji.ac.il

- [1] W. Van Saarloos, V. Vitelli, and Z. Zeravcic, *Soft Matter: Concepts, Phenomena, and Applications* (Princeton University Press, 2024).
- [2] D. R. Nelson, *Defects and geometry in condensed matter physics* (Cambridge University Press, 2002).
- [3] P. M. Chaikin, T. C. Lubensky, and T. A. Witten, *Principles of condensed matter physics*, Vol. 10 (Cambridge university press Cambridge, 1995).
- [4] N. Levy, S. Burke, K. Meaker, M. Panlasigui, A. Zettl, F. Guinea, A. C. Neto, and M. F. Crommie, Strain-induced pseudo-magnetic fields greater than 300 tesla in graphene nanobubbles, *Science* **329**, 544 (2010).
- [5] S. Zhu, J. A. Strosio, and T. Li, Programmable extreme pseudomagnetic fields in graphene by a uniaxial stretch, *Physical review letters* **115**, 245501 (2015).
- [6] E. Sharon, M. Marder, and H. L. Swinney, Leaves, flowers and garbage bags: Making waves, *PLACEHOLDER* (2004).
- [7] Y. Zhang, O. Y. Cohen, M. Moshe, and E. Sharon, Geometrically frustrated rose petals, *Science* **388**, 520 (2025).
- [8] S. Armon, E. Efrati, R. Kupferman, and E. Sharon, Geometry and mechanics in the opening of chiral seed pods, *Science* **333**, 1726 (2011).
- [9] N. Murisic, V. Hakim, I. G. Kevrekidis, S. Y. Shvartsman, and B. Audoly, From discrete to continuum models of three-dimensional deformations in epithelial sheets, *Biophysical journal* **109**, 154 (2015).
- [10] J. Dervaux and M. Ben Amar, Morphogenesis of growing soft tissues, *Physical review letters* **101**, 068101 (2008).
- [11] L. D. Landau, L. Pitaevskii, A. M. Kosevich, and E. M. Lifshitz, *Theory of elasticity: volume 7*, Vol. 7 (Elsevier, 2012).
- [12] E. Efrati, E. Sharon, and R. Kupferman, Elastic theory of unconstrained non-euclidean plates, *Journal of the Mechanics and Physics of Solids* **57**, 762 (2009).
- [13] M. Lewicka, L. Mahadevan, and M. R. Pakzad, The föppl-von kármán equations for plates with, *PLACEHOLDER* (2010).
- [14] P. Ciarletta, G. Pozzi, and D. Riccobelli, The föppl-von kármán equations of elastic plates with initial stress, *Royal Society Open Science* **9**, 220421 (2022).
- [15] D. Nelson, T. Piran, and S. Weinberg, The statistical mechanics of membranes and interfaces, *Statistical Mechanics of Membranes and Surfaces*, 2nd ed.; Nelson, D., Piran, T., Weinberg, S., Eds , 1 (1989).
- [16] A. Pacheco-Sanjuán and R. Batra, Accuracy of föppl-von karman membrane theory for determining elastic constants of monolayer graphene, *International Journal of Mechanical Sciences* **163**, 105154 (2019).
- [17] A. Košmrlj and D. R. Nelson, Response of thermalized ribbons to pulling and bending, *Physical Review B* **93**, 125431 (2016).
- [18] P. Le Doussal and L. Radzihovsky, Anomalous elasticity, fluctuations and disorder in elastic membranes, *Annals of Physics* **392**, 340 (2018).
- [19] D. R. Nelson, Defects in flexible membranes with crystalline order, *Physical Review A* **38**, 1005 (1988).
- [20] T. Zhang, X. Li, and H. Gao, Defects controlled wrinkling and topological design in graphene, *Journal of the Mechanics and Physics of Solids* **67**, 2 (2014).
- [21] K. Guo, M. Suñé, M. L. Kwok, K. J. Hsia, M. Liu, and D. Vella, Localized tension-induced giant folding in unstructured elastic sheets, *Proceedings of the National Academy of Sciences* **122**, e2423439122 (2025).
- [22] M. Leembruggen, J. Andrejevic, A. Kudrolli, and C. H. Rycroft, Computational model of twisted elastic ribbons, *Physical Review E* **108**, 015003 (2023).
- [23] J. Chopin, V. Démery, and B. Davidovitch, Roadmap to the morphological instabilities of a stretched twisted ribbon, *Journal of Elasticity* **119**, 137 (2015).
- [24] E. Cerda and L. Mahadevan, Conical surfaces and crescent singularities in crumpled sheets, *Physical Review Letters* **80**, 2358 (1998).
- [25] E. Cerda and L. Mahadevan, Geometry and physics of wrinkling, *Physical review letters* **90**, 074302 (2003).
- [26] H. Liang and L. Mahadevan, The shape of a long leaf, *Proceedings of the National Academy of Sciences* **106**, 22049 (2009).
- [27] S. Sadik and M. A. Dias, On local kirigami mechanics i: Isometric conical solutions, *Journal of the Mechanics and Physics of Solids* **151**, 104370 (2021).
- [28] M. Moshe, E. Sharon, and R. Kupferman, The plane stress state of residually stressed bodies: A stress function approach, *arXiv preprint arXiv:1409.6594* (2014).
- [29] M. P. do Carmo, *Differential Geometry of Curves and Surfaces* (Prentice-Hall, Englewood Cliffs, NJ, 1976).
- [30] B. Audoly and Y. Pomeau, Finite amplitude buckling of a strip, in *Elasticity and Geometry: From Hair Curls to the Non-linear Response of Shells* (Oxford University Press, Oxford, 2010) Chap. 8, pp. 251–322.
- [31] A. Košmrlj and D. R. Nelson, Response of thermalized ribbons to pulling and bending, *Phys. Rev. B* **93**, 125431 (2016).
- [32] P. Z. Hanakata, S. S. Bhabesh, M. J. Bowick, D. R. Nelson, and D. Yllanes, Thermal buckling and symmetry breaking in thin ribbons under compression, *Extreme Mechanics Letters* **44**, 101270 (2021).
- [33] M. M. Müller, M. B. Amar, and J. Guven, Conical defects in growing sheets, *Phys. Rev. Lett.* **101**, 156104 (2008).
- [34] E. Efrati, L. Pocivavsek, R. Meza, K. Y. C. Lee, and T. A. Witten, Confined disclinations: Exterior versus material constraints in developable thin elastic sheets, *Phys. Rev. E* **91**, 022404 (2015).
- [35] M. Moshe, E. Esposito, S. Shankar, B. Bircan, I. Cohen, D. R. Nelson, and M. J. Bowick, Nonlinear mechanics of thin frames, *Physical Review E* **99**, 013002 (2019).
- [36] K. A. Seffen, Fundamental conical defects: The d-cone, its e-cone, and its p-cone, *Phys. Rev. E* **94**, 013002 (2016).
- [37] R. Kupferman, Bending energy of buckled edge disloca-

- tions, Physical Review E **96**, 063002 (2017).
- [38] R. Kupferman, C. Maor, and D. Padilla-Garza, The will-more energy and curvature concentration, arXiv preprint arXiv:2511.18982 (2025).
- [39] A. Košmrlj and D. R. Nelson, Mechanical properties of warped membranes, PHYSICAL REVIEW E Phys Rev E **88**, 012136 (2013).

## Appendix A: Numerical methods

To determine energy minimizing configurations of elastic sheets prescribed by a reference metric  $\bar{a}$  and reference curvature  $\bar{b}$ , we use a finite element simulation based on a triangulated representation of the sheet. The sheet is modeled as a two dimensional simplicial mesh embedded in  $\mathbb{R}^3$ , where each triangle carries its own local reference metric and reference curvature that encode the preferred in plane distances and out of plane orientations. This geometric formulation extends classical mass spring constructions by assigning rest quantities to triangles rather than to edges.

For each triangular face we reconstruct the intrinsic metric from the current edge lengths. Let  $\mathbf{X}_1, \mathbf{X}_2, \mathbf{X}_3 \in \mathbb{R}^2$  denote the reference coordinates of the face vertices and define  $\mathbf{s}_{ij} = \mathbf{X}_j - \mathbf{X}_i$  as the corresponding reference edge vectors. If  $l_{ij}$  is the current Euclidean length of the edge between vertices  $i$  and  $j$  in  $\mathbb{R}^3$ , then in the parametric domain any tangent vector  $\mathbf{s} = (s_x, s_y)$  satisfies

$$\|\mathbf{s}\|^2 = a_{11}s_x^2 + 2a_{12}s_xs_y + a_{22}s_y^2.$$

Enforcing this on the three reference edges yields the linear system

$$\begin{pmatrix} (s_{23}^x)^2 & 2s_{23}^x s_{23}^y & (s_{23}^y)^2 \\ (s_{31}^x)^2 & 2s_{31}^x s_{31}^y & (s_{31}^y)^2 \\ (s_{12}^x)^2 & 2s_{12}^x s_{12}^y & (s_{12}^y)^2 \end{pmatrix} \begin{pmatrix} a_{11} \\ a_{12} \\ a_{22} \end{pmatrix} = \begin{pmatrix} l_{23}^2 \\ l_{31}^2 \\ l_{12}^2 \end{pmatrix},$$

whose solution determines the metric tensor  $a = \begin{pmatrix} a_{11} & a_{12} \\ a_{12} & a_{22} \end{pmatrix}$ .

To obtain the second fundamental form  $b$  we use the face vertices together with their immediate edge neighbors. Let  $\mathbf{p}_i \in \mathbb{R}^3$ ,  $i = 1, \dots, 6$ , denote these vertices and  $\mathbf{X}_i \in \mathbb{R}^2$  their reference coordinates. The reference center of the face is

$$\mathbf{X}_0 = \frac{1}{3}(\mathbf{X}_1 + \mathbf{X}_2 + \mathbf{X}_3), \quad (x_i, y_i) = \mathbf{X}_i - \mathbf{X}_0,$$

and the current face center and unit normal are

$$\mathbf{P}_0 = \frac{1}{3}(\mathbf{p}_1 + \mathbf{p}_2 + \mathbf{p}_3), \quad \mathbf{n}_0 = \frac{(\mathbf{p}_2 - \mathbf{p}_1) \times (\mathbf{p}_3 - \mathbf{p}_1)}{\|(\mathbf{p}_2 - \mathbf{p}_1) \times (\mathbf{p}_3 - \mathbf{p}_1)\|}.$$

Each vertex provides a height above the face plane through

$$h_i = (\mathbf{p}_i - \mathbf{P}_0) \cdot \mathbf{n}_0.$$

We fit the quadratic height function

$$z(x, y) = c_0 + c_1x + c_2y + \frac{1}{2}Lx^2 + Mxy + \frac{1}{2}Ny^2$$

by enforcing

$$h_i = c_0 + c_1x_i + c_2y_i + \frac{1}{2}Lx_i^2 + Mx_iy_i + \frac{1}{2}Ny_i^2, \quad i = 1, \dots, 6.$$

Solving the resulting  $6 \times 6$  system yields the curvature tensor  $b = \begin{pmatrix} L & M \\ M & N \end{pmatrix}$ .

With the metric and curvature fields available on every triangle, we compute the local stretching and bending energy densities by comparing  $a$  and  $b$  to the prescribed reference fields  $\bar{a}$  and  $\bar{b}$ . The total elastic energy is obtained by summing all triangle contributions with weights given by their reference areas.

This global energy is a smooth function of the vertex positions. Its gradient is assembled by differentiating the discrete metric and curvature expressions with respect to the vertex coordinates.

The minimization begins from an initial configuration and proceeds by iteratively updating the vertex coordinates along the negative gradient of the elastic energy. A line search is applied at each iteration to ensure monotonic decrease of the energy. Convergence is reached once the gradient norm becomes sufficiently small and successive configurations differ only minimally. The resulting shape is a discrete surface whose intrinsic and extrinsic geometry best approximates the prescribed reference data within the limits of the numerical model.

We apply this numerical framework to several thin sheet problems. For each system we first set the elastic moduli  $(Y, \nu)$  and sheet thickness  $h$ , then impose boundary conditions and relax the sheet elastically.

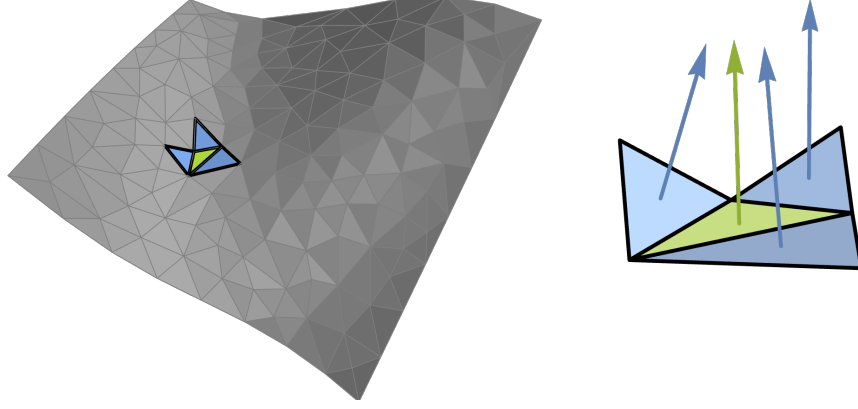


FIG. 3. The metric  $a$  of each triangle is calculated via the lengths of the edges,  $b$  gives the change in the norm and is obtained from height differences of the neighboring triangle vertices.

**Compressed ribbon.** We simulate a ribbon, the vertices along the short edges are fixed to impose clamped boundaries, holding both ends (with some small distance inwards) in a common plane with an end to end separation shorter than the undeformed ribbon length.

**Twisted ribbon.** A ribbon is subjected to a full twist, while the vertices on the short edges are held fixed so that the end to end distance equals the undeformed length.

**Open annulus.** We simulate an annulus, a radial cut is introduced, the two cut boundaries are opened to a prescribed angle by fixing their vertices, and the remainder of the sheet is allowed to relax freely to minimize the elastic energy.

## Appendix B: Deriving the equilibrium equations

To present the complete form of the equilibrium equations as in [12], we assume a reference metric  $\bar{a}$ . The strain tensor is then defined by  $\epsilon_{st} = \frac{1}{2}(a - \bar{a})$ . Based on this, we introduce the stretching and bending stresses, as well as the total stress  $\Sigma$ :

$$\begin{aligned}\sigma^{\alpha\beta} &= 2 \frac{\partial E}{\partial a_{\alpha\beta}} = h A^{\alpha\beta\gamma\delta} \left( \frac{a_{\gamma\delta} - \bar{a}_{\gamma\delta}}{2} \right) \\ m^{\alpha\beta} &= \frac{\partial E}{\partial b_{\alpha\beta}} = \frac{h^3}{12} A^{\alpha\beta\gamma\delta} (b_{\gamma\delta} - \bar{b}_{\gamma\delta}) \\ \Sigma^{\alpha\beta} &= \sigma^{\alpha\beta} + m^{\mu\beta} a^{\gamma\alpha} b_{\mu\gamma}\end{aligned}$$

$\bar{\nabla}$  is the covariant derivative in terms of  $\bar{a}$  (marked above as  $\text{div}_{\bar{a}}$ ), further defining the operator which takes into account both the metric and reference metric meaning  $\text{div}_{\bar{a},a}$  [12]-

$$(\text{div}_{\bar{a},a})_{\mu} T^{\mu\nu} = \bar{\nabla}_{\mu} T^{\mu\nu} + \left( \Gamma_{\alpha\beta}^{\nu} - \bar{\Gamma}_{\alpha\beta}^{\nu} \right) T^{\alpha\beta} \quad (\text{B1})$$

The full energy functional is of the form (Eq (1)),

minimizing in terms of the configuration results with the equilibrium equations [12]:

$$0 = (\text{div}_{\bar{a},a})_{\beta} (\Sigma^{\alpha\beta}) + (\text{div}_{\bar{a},a})_{\beta} (m^{\mu\beta}) a^{\gamma\alpha} b_{\gamma\mu} \quad (\text{B2})$$

$$0 = \bar{\nabla}_{\alpha} ((\text{div}_{\bar{a},a})_{\beta} (m^{\alpha\beta})) - \Sigma^{\alpha\beta} b_{\alpha\beta} \quad (\text{B3})$$

Next, we will look at the leading orders of these equations in the case where  $\bar{b} = 0$ . We note the Christoffel symbols term scales like the strain:  $\Gamma - \bar{\Gamma} \sim \epsilon_{st}$ . In the FvK scaling regime, where the stretching and bending energy terms are

of the same order  $\epsilon_{\text{st}} \sim \frac{h^2}{\ell^2}$ ,  $\epsilon_{\text{bn}} \sim \frac{h}{\ell^2}$  with the length-scale  $\ell$  depends on the specific system, the equilibrium equations reduce to:

$$0 = \bar{\nabla}_\beta(\sigma^{\alpha\beta}) \quad (\text{B4})$$

$$0 = \bar{\nabla}_\alpha \bar{\nabla}_\beta m^{\alpha\beta} - \sigma^{\alpha\gamma} b_{\alpha\gamma} \quad (\text{B5})$$

Allowing a general reference curvature  $\bar{b} \neq 0$ , means we must return to the full equilibrium equations -Eqs (B2),(B3). In order to simplify the equations for certain scalings we must take into account large bending can exist even for small bending strain. For all scalings, the equilibrium equations have extra terms from  $\bar{b}$ . In the past a reference height profile was assumed to address such configurations[39], a general reference curvature does not have compatibility requirements, and we leave this for future work.

### Appendix C: Boundary conditions

The transition from the classical FvK height function  $f$  to the curvature potential  $\psi$  in the geometric formulation causes the same difficulties as the earlier shift from in-plane displacement vectors to the Airy stress potential  $\chi$ ; in both cases, one loses the immediate clarity regarding the boundary conditions.

The free boundary terms of the equilibrium equations Eqs (B3)-(3) are derived in [12] and given by:

$$0 = \Sigma^{\mu\nu} n_\nu \quad (\text{C1})$$

$$0 = m^{\alpha\beta} n_\alpha n_\beta \quad (\text{C2})$$

$$0 = (\text{div}_{a,\bar{a}})_\alpha (m^{\alpha\beta}) n_\beta \quad (\text{C3})$$

Which define the force on the boundary (C1) and the curvature torque (C2),(C3).

Here, too, for the FvK scaling ( $\epsilon_{\text{st}} \sim h^2$ ,  $\epsilon_{\text{bn}} \sim h$ ) we take the leading orders of each equation, resulting with:

$$0 = \sigma^{\mu\nu} n_\nu \quad (\text{C4})$$

$$0 = m^{\alpha\beta} n_\alpha n_\beta \quad (\text{C5})$$

$$0 = (\bar{\nabla}_\alpha m^{\alpha\beta}) n_\beta \quad (\text{C6})$$

There an alternative way to define the boundary terms, rather then looking at the force and torques we look at the actual configuration- using the Weingertan equations explicitly to require boundary conditions.

The configuration itself  $\Phi$  is found from the weingertan equations, given the first and second fundamental forms.

$$\partial_\mu \partial_\nu \Phi = \Gamma_{\mu\nu}^\alpha \partial_\alpha \Phi + b_{\mu\nu} \hat{n} \quad (\text{C7})$$

$$\partial_\mu \hat{n} = -a^{\alpha\beta} b_{\mu\alpha} \partial_\beta \Phi \quad (\text{C8})$$

We will show an explicit example of how to do so.

**Compressed ribbon boundary conditions.** In this problem the results admit uniform strain, meaning  $a$  is not dependent on the coordinates, therefore the christoffel symbols admit  $\Gamma = 0$ , reducing the Weingertan equations to:

$$\partial_u \hat{n} = -\psi'' \partial_u \Phi \quad (\text{C9})$$

$$\partial_u \partial_u \Phi = \psi'' \cdot \hat{n} \quad (\text{C10})$$

As we solved with no dependence on the coordinate  $v$  along the short side of the ribbon  $\psi(u, v) = \psi(u) = A \cos(\frac{2\pi}{L} u)$  the mode, is the lowest mode which gives flat (clamped) boundaries, this leads to the ODE:

$$\hat{n}''(u) - \frac{\psi'''}{\psi''} \hat{n}'(u) + (\psi'')^2 \hat{n}(u) = 0 \quad (\text{C11})$$

for the configuration in 3D we choose an arbitrary direction and the b.c we impose are  $\hat{n}(\pm \frac{L}{2}) = (0, 0, 1)$  solving the equation, the normal then gets the shape:  $(\sin(\frac{c}{k} \sin(ku)), 0, \cos(\frac{c}{k} \sin(ku)))$

using Eq (C9) to calculate the distance between the 2 edges-

$$\Phi(u = \frac{\ell}{2}) - \Phi(u = -\frac{\ell}{2}) = \int_{-\frac{\ell}{2}}^{\frac{\ell}{2}} \Phi' du = \int_{-\frac{\ell}{2}}^{\frac{\ell}{2}} -\frac{\partial_u \hat{n}}{\psi''} du = \left(0, 0, L J_0 \left(\frac{cL}{2\pi}\right)\right) \quad (\text{C12})$$

$J_0$  is a Bessel function, this gives the distance between the short sides of the ribbon and allows us to impose boundary conditions via the parameter  $c$ .



### Appendix D: The isometric limit

To solve this problem we will look back at the general elastic energy (1), now at the thin limit meaning  $h \rightarrow 0$ , which enforces  $a = \bar{a}$ . Minimizing the bending energy must be supplemented with the compatibility equations (2). Writing  $b$  in terms of CP ensures one of the compatibility terms the other must be added to the energy as a Lagrange multiplier.

$$U = \int \left[ \frac{h^3}{24} A^{\alpha\beta\gamma\delta} b_{\alpha\beta} b_{\gamma\delta} - \lambda \left( \det \left( \frac{b}{\bar{a}} \right) - \bar{K}_G \right) \right] dS \quad b_{\alpha\beta} = \bar{\nabla}_{\alpha\beta} \psi \quad (D1)$$

The resulting bulk equation via variation of  $\psi$  the curvature potential gives:

$$B \bar{\Delta} \bar{\Delta} \psi = \Lambda \cdot b \quad \Lambda^{\alpha\beta} = \frac{\epsilon^{\alpha\beta}}{\sqrt{\bar{a}}} \frac{\epsilon^{\alpha\beta}}{\sqrt{\bar{a}}} \bar{\nabla}_{\mu\nu} \lambda \quad (D2)$$

where  $\lambda$  act the like the SP  $\chi$ . In addition to this equation we have the condition from the Lagrange multiplier  $\det(\bar{a}^{-1}b) = \bar{K}_G$

### Appendix E: Twisted ribbon derivation

When looking at a ribbon we assume an almost 2D surface where one dimension is much larger than the others  $(u, v, w) \in [-\frac{L}{2}, \frac{L}{2}] \times [-\frac{w}{2}, \frac{w}{2}] \times [-\frac{h}{2}, \frac{h}{2}]$  where  $h \ll w \ll L$  with  $\bar{a} = \text{Id}$ ,  $\bar{b} = 0$ .

We will find solutions for FVK equations under this assumption and additionally assuming that there is no explicit dependence on the long coordinate  $u \Rightarrow \sigma = \sigma(v)$  and  $b = b(v)$  and no force on the applied on the long side of the ribbon ( $[\sigma \cdot n]_{(u,v=\pm \frac{w}{2})} = 0$ ). The most general shape of such a solution is

$$f(u, v) = f_1 u^2 + f_2 uv + \tilde{f}(v) \quad (E1)$$

Next, we will look at the solutions to FVK equations given this shape of functions

$$\chi(u, v) = \frac{\chi_0}{2} u^2 + \chi_1 uv + \chi_2(v) \quad \sigma = \begin{pmatrix} \chi_2''(v) & -\chi_1 \\ -\chi_1 & \chi_0 \end{pmatrix} \quad (E2)$$

and the boundary term  $[\sigma \cdot n]_{(u,v=\pm \frac{w}{2})} = 0$  gives  $\chi_0 = \chi_1 = 0$

$$\psi(u, v) = \frac{\psi_0}{2} u^2 + \psi_1 uv + \psi_2(v) \quad b = \begin{pmatrix} \psi_0 & \psi_1 \\ \psi_1 & \psi_2''(v) \end{pmatrix} \quad (E3)$$

substituting into the FVK equations gives simplified equations-

$$\chi_2''''(v) = Y(\psi_0 \psi_2''(v) - \psi_1^2) \quad (E4)$$

$$\psi_2''''(v) = \psi_0 \chi_2''(v) \quad (E5)$$

when we choose (C2) to be constant then  $\psi_2(v) = \frac{1}{2} \psi_2 v^2$  then  $\det(b) = \text{const}$  and from (E4) -  $\chi_2(v) = \frac{1}{2} c_2 v^2 + \frac{1}{6} c_3 v^3 + \frac{1}{24} c_4 v^4$ . Assuming symmetry on both sides of the mid line  $c_3 = 0$  then from from (E5):  $0 = \psi_0 (c_2 + \frac{1}{2} c_4 v^2)$  we get  $\psi_0 = 0$ . Summing up:

$$\begin{aligned} \chi(u, v) &= \frac{c}{2} v^2 - \frac{Y \psi_1^2}{24} v^4 \\ \psi(u, v) &= \psi_1 uv + \frac{\psi_2}{2} v^2 \end{aligned} \quad (E6)$$

finally, 3 parameters control the configuration determined by the boundary conditions:

$$[\sigma \cdot n]_{v=\pm w/2} = 0, \quad [\sigma \cdot n]_{u=\pm \ell/2} = c - \frac{E \psi_1}{2} v^2, \quad (E7)$$

$$[m \cdot n \cdot n]_{v=\pm w/2} = \frac{h^3 E}{24(1+\nu)(1-\nu)} \psi_2, \quad [m \cdot n \cdot n]_{u=\pm \ell/2} = \frac{h^3 E \nu}{24(1+\nu)(1-\nu)} \psi_2, \quad (E8)$$

$$[\nabla(m) \cdot n]_{v=\pm w/2} = 0, \quad [\nabla(m) \cdot n]_{u=\pm \ell/2} = 0. \quad (E9)$$

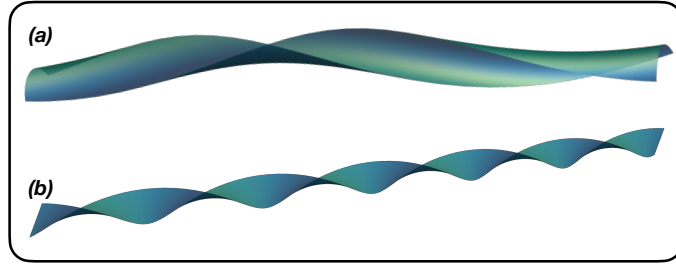


FIG. 4. Resulting configurations of a twisted ribbon: Panel (a) shows a ribbon with dimensions  $1 \times 10$  for  $\psi_1 = \frac{2\pi}{10}$ ,  $c = 0$ , and  $\psi_2 = 3$ ; panel (b) corresponds to a ribbon with dimensions  $1 \times 100$  with  $\psi_1 = \frac{6\pi}{100}$ ,  $c = 0$ , and  $\psi_2 = 0$ .

where  $c$  controls the total length of the ribbon,  $\psi_1$  is the twist per unit length and  $\psi_2$  gives curvature along the short side of the ribbon.

### Scaling of $b$

From the requirement  $\epsilon_{\text{st}} \sim h\epsilon_{\text{bn}}$ , meaning the stretching and bending energy are comparable, we get the scaling of  $b$ . In this case we will get the conditions looking at the energy density of each term for  $\psi = \psi_1 uv$  and  $\chi = -\frac{Y\psi_1^2}{24}v^4$ :

$$\mathcal{U}_S \sim h v^4 \psi_1^4 \quad \mathcal{U}_B \sim h^3 \psi_1^2 \quad (\text{E10})$$

where  $v \in [-\frac{W}{2}, \frac{W}{2}]$ , for them to be of the same magnitude  $\psi_1 \sim \frac{h}{W^2}$ . This gives a maximum to the number of twists per unit length  $\psi$  depending on the system width.

### Appendix F: Compressed ribbon

For a ribbon with dimension  $(u, v, w) \in [-\frac{L}{2}, \frac{L}{2}] \times [-\frac{w}{2}, \frac{w}{2}] \times [-\frac{h}{2}, \frac{h}{2}]$  where  $h \ll w \ll L$  with  $\bar{a} = \text{Id}$ ,  $\bar{b} = 0$ . with flat reference terms  $\bar{a} = \begin{pmatrix} 1 & 0 \\ 0 & 1 \end{pmatrix}$   $\bar{b} = 0$ ; the general solutions which solve the equilibrium equations both in the FvK limit and in the isometric limit (in that case  $\chi$  takes the position of a Lagrange multiplier insuring zero Gaussian curvature (see App. D)) [30]:

$$\chi(u, v) = \frac{Yh^3}{24(1-\nu^2)}\kappa^2 u^2 + c_1 uv + c_2 v^2, \quad \psi(u, v) = A \cos(\kappa u) + B \sin(\kappa u), \quad (\text{F1})$$

$A, B, \kappa$  must obey the boundary condition, in our case we force the short edges of the ribbon to stay flat meaning  $B = 0$  and  $\kappa = \frac{2\pi}{L}n$ . For small loads we expect to find the first mode— $n = 1$ .  $A$  is then determined by the distance between the short edges (see App. C).

### Appendix G: Bent sliced annulus

We consider a flat disc with a radial cut, which allows the disc to be opened by prescribing two types of boundary control parameters: (i) the angle between the two open edges and their relative tilt (the  $\psi$  parameters), and (ii) the alignment of these edges (the  $\chi$  parameters). Figure 5 illustrates several examples of such configurations.

A bending potential  $\psi$  which allows curvature only on the azimuthal direction has the shape:  $\psi(r, \theta) = rf(\theta)$

$$\psi(r, \theta) = r(c_1 \theta \cos \theta + c_2 \theta \sin \theta + c_3 \cos \theta + c_4 \sin \theta). \quad (\text{G1})$$

The SP  $\chi$  which solves the equilibrium equations is of the shape:

$$\chi(r, \theta) = a_1 \cos(2\theta) + a_2 \sin(2\theta) + r\theta(b_1 \cos \theta + b_2 \sin \theta) \quad (\text{G2})$$

where we ignore extra term which do not contribute to the stress. We focus on boundary conditions that admit stretching-free configurations. There exist boundary conditions which require no stress  $a = \bar{a} = \begin{pmatrix} 1 & 0 \\ 0 & r^2 \end{pmatrix}$ . The boundary conditions follow from the Weingarten equations (see Appendix C). We validated these results using finite-element

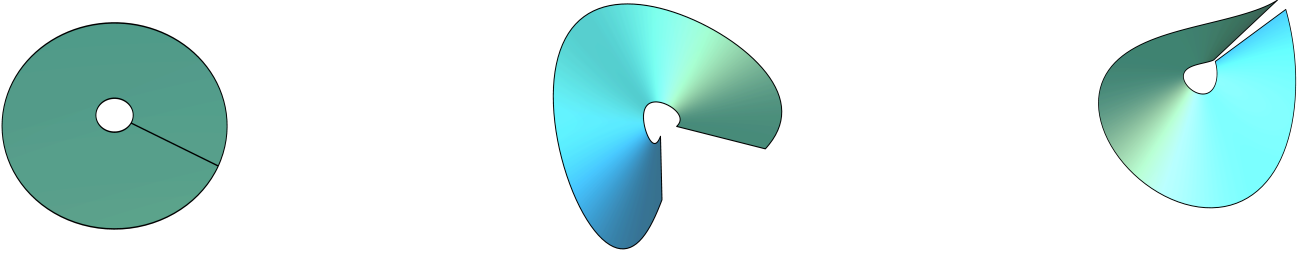


FIG. 5. Opening an annulus with a radial cut. The resulting configuration is determined by the opening angle and tilt of the cut edges. Because the annulus is a thin flat sheet with zero Gaussian curvature, we search for stretching-free configurations generated purely by bending via the FvK equations.

simulations for two representative curvature tensors:

$$b = \begin{pmatrix} 0 & 0 \\ 0 & cr \sin \theta \end{pmatrix}, \quad b = \begin{pmatrix} 0 & 0 \\ 0 & cr \cos \theta \end{pmatrix}.$$

Simulations of this kind are shown in Fig. 2(b) and Fig. 6. Here, in Fig. 6 the Gaussian and mean curvature fields from the simulations are compared with the analytic CP predictions for  $\chi = 0$ . The configuration is colored by Gaussian curvature (expected to vanish in the isometric limit), along with maps of mean curvature and their deviations.

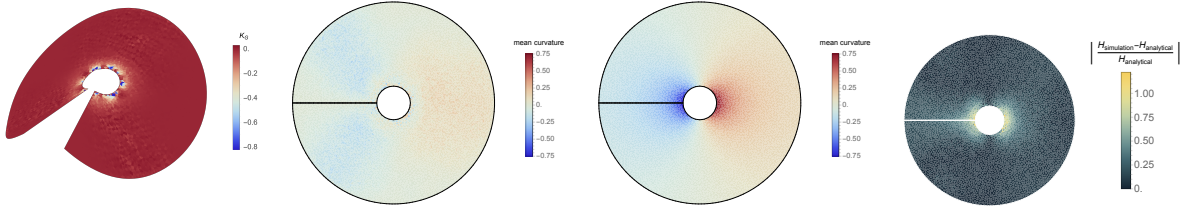


FIG. 6. Finite-element simulation corresponding to the bending potential  $\psi(r, \theta) = 0.4 r \theta \sin \theta$ . Shown are Gaussian curvature, simulated mean curvature, analytic mean curvature, and normalized deviation. As in the previous case, the largest deviations occur near the inner boundary.